

Molecular gas chemistry in AGN

I. The IRAM 30 m survey of NGC 1068

A. Usero^{1,2}, S. García-Burillo¹, A. Fuente¹, J. Martín-Pintado³, and N. J. Rodríguez-Fernández⁴

¹ Observatorio Astronómico Nacional (OAN), C/ Alfonso XII 3, 28014 Madrid, Spain

² Instituto de Matemáticas y Física Fundamental, CSIC, C/ Serrano 113bis, 28006 Madrid, Spain

³ Instituto de Estructura de la Materia, DAMIR-CSIC, C/ Serrano 121, 28006 Madrid, Spain

⁴ LERMA (UMR 8112), Observatoire de Paris, 61 Av. de l'Observatoire, 75014 Paris, France

Received 1 December 2003 / Accepted 5 February 2004

Abstract. There is observational evidence that nuclear winds and X-rays can heavily influence the physical conditions and chemical abundances of molecular gas in the circumnuclear disks (CND) of Active Galactic Nuclei (AGN). In this paper we probe the chemical status of molecular gas in the CND of NGC 1068, a prototypical Seyfert 2 galaxy. Precedent claims that the chemistry of molecular gas in the nucleus of NGC 1068 is *abnormal* by galactic standards were based on the high HCN/CO luminosity ratio measured in the CND. Results from new observations obtained in this survey have served to derive abundances of molecular species such as SiO, CN, HCO⁺, HOC⁺, H¹³CO⁺ and HCO. These estimates are complemented by a re-evaluation of molecular abundances for HCN, CS and CO, based on previously published single-dish and interferometer observations of NGC 1068. We report on the first detection of SiO emission in the CND of NGC 1068. The estimated large abundance of SiO in the CND, $X(\text{SiO}) \sim (5-10) \times 10^{-9}$, cannot be attributed to shocks related to star formation, as there is little evidence of a recent starburst in the nucleus of NGC 1068. Alternatively, we propose that silicon chemistry is driven by intense X-ray processing of molecular gas. We also report on the first extragalactic detection of the reactive ion HOC⁺. Most remarkably, the estimated HCO⁺/HOC⁺ abundance ratio in the nucleus of NGC 1068, $\sim 30-80$, is the smallest ever measured in molecular gas. The abundances derived for all molecules that have been the subject of this survey are compared with the predictions of models invoking either oxygen-depletion or X-ray chemistry in molecular gas. Our conclusions favour an overall scenario where the CND of NGC 1068 has become a giant X-ray Dominated Region (XDR).

Key words. galaxies: individual: NGC 1068 – galaxies: Seyfert – galaxies: nuclei – galaxies: ISM – ISM: abundances – radio lines: galaxies

1. Introduction

Active Galactic Nuclei (AGN) are able to inject vast amounts of energy into their host galaxies, carried by strong radiation fields and rapidly moving jets. It is predictable that AGN should have a disruptive influence on the gas reservoir near their central engines. There is multi-wavelength observational evidence that the general properties of neutral interstellar matter in AGN differ from those of quiescent star-forming disks and starburst galaxies (Genzel et al. 1998; Laurent et al. 2000). In particular, molecular gas close to the central engines of active galaxies can be exposed to a strong X-ray irradiation. While the accretion disks of AGN are strong UV emitters, the bulk of the UV flux can be attenuated by neutral gas column densities of only $N(\text{H}) \sim 10^{21} \text{ cm}^{-2}$. Hard X-ray photons (2–10 keV) can penetrate neutral gas column densities out to $N(\text{H}) \sim 10^{23}-10^{24} \text{ cm}^{-2}$, however. Therefore, X-ray dominated regions (XDR) could become the dominant sources

of emission for molecular gas in the harsh environment of circumnuclear disks (CND) of AGN, as originally argued by Maloney et al. (1996).

First observational evidence that the physical and chemical properties of molecular gas in the CND of AGN depart from “normality” came from the single-dish and interferometer observations of HCN and CO emission in NGC 1068 (Tacconi et al. 1994; Sternberg et al. 1994). This prototypical Seyfert 2 galaxy hosts a circumnuclear starburst ring of $\sim 2.5-3 \text{ kpc}$ -diameter (see Fig. 1); the ring delimits a 2.3 kpc stellar bar detected by Scoville et al. (1988) in the NIR. The strong emission detected in the 1–0 and 2–1 CO lines coming from the starburst ring corroborates that massive star formation is fed by a significant gas reservoir (Planesas et al. 1989, 1991; Helfer & Blitz 1995; Schinnerer et al. 2000). Significant CO emission arises also from a 200 pc CND of $M(\text{H}_2) \sim 5 \times 10^7 M_\odot$ (inferred using a $N(\text{H}_2)/I(\text{CO})$ conversion factor of $2.2 \times 10^{20} \text{ cm}^{-2} (\text{K km s}^{-1})^{-1}$, from Solomon & Barrett 1991). The CND, partly resolved into two knots, surrounds

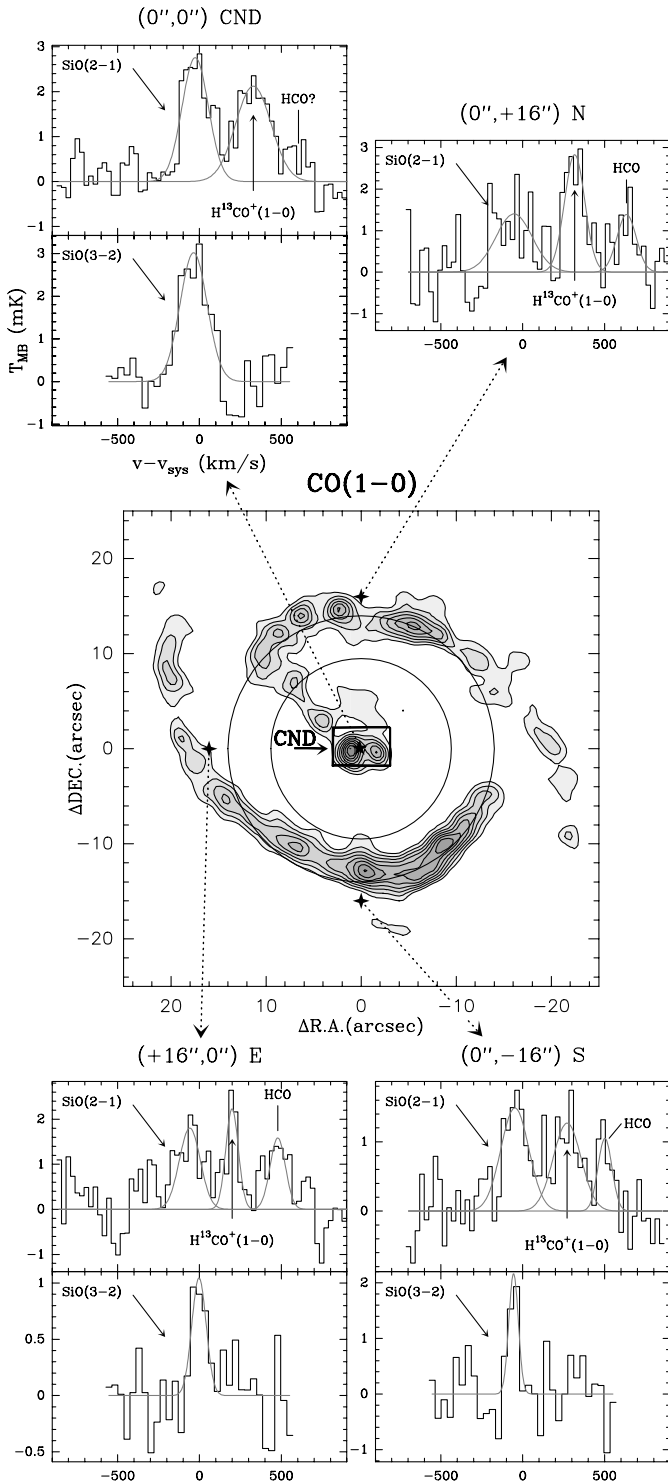


Fig. 1. Emission spectra of the 2–1 and 3–2 lines of SiO detected in the inner 3 kpc of NGC 1068. Four starred markers, overlaid on the CO(1–0) integrated intensity map of Schinnerer et al. (2000), highlight the central positions of the beams in the disk where we searched for SiO emission: the central offset (0'', 0'') coincides with the position of the AGN, given by the S1 compact radio-source of Gallimore et al. (1996b) ($\alpha_{2000} = 02^{\text{h}}42^{\text{m}}40^{\text{s}}.71$, $\delta_{2000} = -00^{\circ}00'47.9''$), while offsets N, S and E probe the SiO emission over the starburst ring. Emission in the H¹³CO⁺(1–0) and HCO(1–0) lines is detected in the CND and over the starburst ring. The circles represent the beam sizes at 130.3 GHz (19'') and 86.8 GHz (28'').

the position of the active nucleus identified as the compact radio-source S1 in the map of Gallimore et al. (1996a). Most remarkably, the CND is prominent in HCN emission (Tacconi et al. 1994). According to the analysis of Sternberg et al. (1994), the high HCN/CO intensity ratio measured by Tacconi et al. (1994) ($\sim 1-10$) leads to an abnormally high HCN/CO abundance ratio in the nucleus of NGC 1068: $N(\text{HCN})/N(\text{CO}) \sim \text{a few } 10^{-3}-10^{-2}$, i.e., the highest ratio ever found in the centre of any galaxy.

Different explanations have been advanced to quantify the possible link between the anomalous HCN chemistry and the presence of an active nucleus in NGC 1068. The selective depletion of gas-phase oxygen in the dense molecular clouds would explain the high HCN-to-CO abundance ratio (Sternberg et al. 1994; Shalabiea & Greenberg 1996). The same oxygen depletion scheme predicts a lower-than-normal abundance of all oxygen-bearing species. Alternatively, an increased X-ray ionization of molecular clouds near the AGN could enhance the abundance of HCN (Lepp & Dalgarno 1996). Furthermore, X-rays could evaporate small (~ 10 Å) silicate grains, increasing the fraction in gas phase of all refractory elements and subsequently enhancing the abundance of some molecules (e.g., SiO) in X-ray irradiated molecular gas (Voit 1991; Martín-Pintado et al. 2000). While the aforementioned scenarios succeed to reproduce the measured enhancement of HCN relative to CO in NGC 1068, their predictions about the abundances of other molecular species differ significantly. The lack of tight observational constraints for these models, prompted by the first mm-observations made in NGC 1068, has hampered thus far the choice of an optimum scenario, however.

In this paper we discuss the results of a molecular survey made in NGC 1068 with the IRAM 30 m mm-telescope. NGC 1068 is the optimum target to quantify the feed-back of activity and star formation on the chemistry of molecular gas. Furthermore, the spatial resolution of the 30 m telescope is well suited to discern between the emission coming from the star forming ring and that coming from the CND. We discuss the results obtained from new mm-observations of 6 molecular species. The list includes: SiO($v = 0$, $J = 2-1$ and $J = 3-2$), HCO($J = 3/2-1/2$, $F = 2-1$), H¹³CO⁺($J = 1-0$), HCO⁺($J = 1-0$), HOC⁺($J = 1-0$) and CN($N = 2-1$). For comparison purposes, we include in our analysis the results from previous single-dish and interferometer observations of CO ($J = 1-0$ and 2–1 from Schinnerer et al. 2000; $J = 4-3$ from Tacconi et al. 1994), HCN ($J = 1-0$ and 4–3) (Tacconi et al. 1994) and CS ($J = 2-1$) (Tacconi et al. 1997). This data base has served for estimating the abundances of eight molecular species in the CND of NGC 1068 using LVG model calculations. The inferred abundances are compared with the predictions of models invoking either oxygen-depletion or X-ray chemistry in molecular gas. We present in Sect. 2 the 30 m observations made for this survey as well as the data compiled from previous works on NGC 1068. Section 3.1 presents the results obtained from our SiO study and their implications for the CND chemistry. Section 3.2 is devoted to discuss the chemistry of the HOC⁺/HCO⁺ active ions. The molecular gas inventory of the CND is globally presented and discussed in Sect. 4.

Table 1. Main parameters of the new 30 m observations (*top*). Typical receiver and system temperatures are shown as T_{rec} and T_{sys} , respectively. We also show the relevant parameters for previous observations used in this work (*bottom*). See original references for details.

New observations					
Line	Freq. (GHz)	Obs. dates	Beam (")	η_{B}	$T_{\text{rec}}/T_{\text{sys}}$ (K)
H ¹² CO(3/2–1/2, 2–1)	86.670	Jun. 00/Aug. 02	28	0.82	70/130
H ¹³ CO ⁺ (1–0)	86.754	Jun. 00/Aug. 02	28	0.82	70/130
SiO(2–1)	86.847	Jun. 00/Aug. 02	28	0.82	70/130
H ¹² CO ⁺ (1–0)	89.189	Jan. 01/May 01	27	0.81	60/120
HO ¹² C ⁺ (1–0)	89.487	Jan. 01/May 01	27	0.81	60/120
SiO(3–2)	130.269	Jun. 00/Aug. 02	19	0.77	125/225
CN(2–1)	226.875	Aug. 02	11	0.58	120/390
Previous data					
Line	Freq. (GHz)	Telescope	Reference paper		
HCN(4–3)	354.505	JCMT	Tacconi et al. (1994)		
CO(4–3)	461.041	JCMT	Tacconi et al. (1994)		
HCN(1–0)	89.088	IRAM PdBI	Tacconi et al. (1994)		
CS(2–1)	97.981	IRAM PdBI	Tacconi et al. (1997)		
CO(1–0)	115.271	IRAM PdBI	Schinnerer et al. (2000)		
CO(2–1)	230.538	IRAM PdBI	Schinnerer et al. (2000)		

We discuss in Sect. 5 the interpretation of these results in the framework of different chemistry models and summarize the main conclusions of this work in Sect. 6.

2. Observations

The observations have been carried out in four sessions from January 2000 to August 2002 with the IRAM 30 m radiotelescope at Pico Veleta (Spain). We used 3 SIS receivers tuned in single-sideband mode in the 1 mm, 2 mm and 3 mm bands to observe several transitions of the molecular species shown in Table 1, which summarizes the relevant parameters of these observations. We have obtained single-pointed spectra toward the nucleus of NGC 1068 for all the molecules with the exception of SiO, HCO and H¹³CO⁺, for which we obtained partial maps by observing three additional positions on the starburst ring (see Sect. 3.1). The line temperature scale used by default throughout the paper is T_{MB} , i.e., main brightness temperature. T_{MB} is related to antenna temperature, T_{A}^* , by $T_{\text{A}}^* = T_{\text{MB}} \times \eta_{\text{B}}$; the values assumed for η_{B} are listed in Table 1. When explicitly stated, T_{MB} temperatures are corrected by a source coupling factor, f_{S}^1 ; this factor accounts for the estimated dilution of the source within the beam. To improve the stability of spectral baselines, the observations have been carried out in beam-switching mode, with an azimuthal switch of $\pm 4'$ with a frequency of 0.5 Hz. Only linear polynomials were used in the baseline correction.

In this paper we also use the data from previously published HCN, CS and CO observations of NGC 1068 made with

¹ Correction for dilution: $T \rightarrow f_{\text{S}}T$ with $f_{\text{S}} = \Omega_{\text{beam}}/\Omega_{\text{S}}$, where Ω_{beam} is the beam area and Ω_{S} the area of the emitting region estimated from the CO(1–0) interferometer map.

the IRAM Plateau de Bure Interferometer-PdBI (HCN(1–0): Tacconi et al. 1994; CS(2–1): Tacconi et al. 1997; CO(1–0) and CO(2–1): Schinnerer et al. 2000). Complementary observations of high J transitions ($J = 4–3$) of CO and HCN, taken at James Clerk Maxwell Telescope-JCMT (Tacconi et al. 1994), are also included. The main parameters of these observations are listed in Table 1.

Hereafter, we will assume a distance to NGC 1068 of 14.4 Mpc (Bland-Hawthorn et al. 1997). This implies $1'' = 72$ pc. The assumed heliocentric systemic velocity is $v_{\text{sys}} = 1137$ km s^{−1} (from NASA/IPAC Extragalactic Database (NED)).

3. The IRAM 30 m survey of NGC 1068

3.1. SiO emission in NGC 1068

NGC 1068 was originally part of a larger extragalactic survey searching for SiO emission in starbursts (Usero et al. 2003 in prep.). Different mechanisms have been found thus far to explain the enhancement of SiO abundances in molecular gas in galaxies: either related to recent star formation (NGC 253: García-Burillo et al. 2000), to the disruption of galaxy disks by large-scale shocks (M 82: García-Burillo et al. 2001) or to the X-ray irradiation of molecular clouds (Milky Way: Martín-Pintado et al. 2000).

We show in Fig. 1 the 4 positions over the NGC 1068 disk where we searched for SiO emission. To better constrain the physical conditions of the gas, we have observed simultaneously the $J = 2–1$ and $J = 3–2$ rotational transitions of SiO. SiO(2–1) emission is detected at every offset, while SiO(3–2), very prominent in the CNB, is detected in 2 out of the 3 positions mapped over the ring. The observing grid was

Table 2. Parameters of gaussian fits to the SiO/H¹³CO⁺/HCO lines observed in NGC 1068. Errors (in brackets) are 1- σ . For the non-detection of SiO(3–2) in the *N* position we give a 3- σ upper limit.

Position	Line	I (K km s ⁻¹)	T_{peak} (mK)	$v - v_{\text{sys}}$ (km s ⁻¹)	Δv (km s ⁻¹)
CND (0'', 0'')	SiO(2–1)	0.56 (0.05)	2.8	–26 (10)	189 (22)
	SiO(3–2)	0.60 (0.06)	3.0	–36 (10)	190 (19)
	H ¹³ CO ⁺ (1–0)	0.57 (0.07)	2.1	9 (13)	254 (38)
S (0'', –16'')	SiO(2–1)	0.32 (0.04)	1.5	–48 (9)	200 (13)
	SiO(3–2)	0.17 (0.04)	2.2	–57 (9)	69 (18)
	H ¹³ CO ⁺ (1–0)	0.27 (0.04)	1.3	–48 (13)	200 (13)
	HCO(3/2–1/2, 2–1)	0.11 (0.03)	1.1	–107 (13)	100 (13)
N (0'', +16'')	SiO(2–1)	0.39 (0.08)	1.4	–53 (29)	261 (52)
	SiO(3–2)	<0.25
	H ¹³ CO ⁺ (1–0)	0.44 (0.07)	2.8	–3 (11)	145 (27)
	HCO(3/2–1/2, 2–1)	0.20 (0.07)	1.4	26 (23)	138 (60)
E (+16'', 0'')	SiO(2–1)	0.28 (0.04)	1.8	–60 (19)	150 (13)
	SiO(3–2)	0.11 (0.04)	1.1	1 (19)	103 (36)
	H ¹³ CO ⁺ (1–0)	0.21 (0.03)	2.2	–122 (9)	90 (13)
	HCO(3/2–1/2, 2–1)	0.18 (0.04)	1.6	–130 (20)	110 (13)

chosen to discriminate between SiO emission coming from the starburst ring (N[0'', +16''], E[+16'', 0''] and S[0'', –16'']) and that coming from the circumnuclear disk (CND[0'', 0'']). Parameters of the gaussian fits to the lines detected are listed in Table 2.

3.1.1. Emission in the starburst ring

These observations show that SiO emission is widespread in the starburst ring of NGC 1068. Where detected over the ring, SiO(3–2) lines are narrower than SiO(2–1) lines. This result can be explained if, contrary to the compactness of SiO emission in the CND (see below), the emission of SiO on the ring extends significantly beyond a single SiO(3–2) beam. Within the errors, the $I(\text{SiO}(3-2))/I(\text{SiO}(2-1))$ integrated intensity ratios are ~ 0.5 in the two positions with detection of the 2 mm line. These ratios are slightly lowered to 0.4 ± 0.1 if we apply a correction due to the different coupling factors of the 3–2 and 2–1 beams with the source (correcting for dilution of the nearly one-dimensional elongated arm inside the beams, i.e., by a factor $\sim 19''/28''$).

There are two precedents for the detection of large-scale SiO emission associated with ongoing star formation: NGC 253 (García-Burillo et al. 2000) and M 82 (García-Burillo et al. 2001). The derived enhancement of SiO abundances ($X(\text{SiO}) \sim \text{a few } 10^{-10} - 10^{-9}$) takes place on scales of several hundred pc in these starbursts and has been interpreted as a signature of shocks driven by YSO, SN explosions and/or density waves. In the starburst ring of NGC 1068, a significant fraction of the stellar population ($\sim 40\%$ of the total optical light; González-Delgado et al. 2001) has typical ages $\leq 10^7$ yr. This supports that a recent short burst of star formation has occurred coevally throughout the ring on a time-scale of $\sim 10^6$ yr (Davies et al. 1998).

Beside the detection of the 1–0 line of H¹³CO⁺ (see Fig. 1), which is 93 MHz redshifted with respect to the SiO(2–1)

line, we have detected the emission of the strongest hyperfine component ($F = 2-1$) of the $J = 3/2-1/2$ line of HCO over the starburst ring. Observations of HCO in galactic clouds suggest that the abundance of this molecule is enhanced in Photon Dominated Regions (PDR). More recently, García-Burillo et al. (2002) have reported on the detection of widespread HCO emission in the nuclear starburst of M 82, where it traces the propagation of PDR chemistry in the disk. Based on studies of HCO emission in Galactic PDR (Schenewerk et al. 1986, 1988), it is plausible to suppose that the HCO lines should be optically thin also in the starburst ring of NGC 1068. For H¹³CO⁺ we also consider optically thin emission and the same excitation temperature as that assumed for HCO. These are reasonable guesses, especially for T_{ex} , as the two molecules have similar critical densities for the examined transitions. In this case, the calculation of the HCO-to-H¹³CO⁺ column density ratio is straightforward using the expression (Schenewerk et al. 1988):

$$\frac{N(\text{HCO})}{N(\text{H}^{13}\text{CO}^+)} \simeq \frac{12}{5} \frac{I_{\text{HCO}} A_{\text{HCO}}^{-1}}{I_{\text{H}^{13}\text{CO}^+} A_{\text{H}^{13}\text{CO}^+}^{-1}} \quad (1)$$

where N is the total column density, I is the integrated intensity, and A is the Einstein coefficient of the transition. We infer an average value for $N(\text{HCO})/N(\text{H}^{13}\text{CO}^+)$ of ~ 8 . Adopting an average fractional abundance for H¹³CO⁺ of 10^{-10} (García-Burillo et al. 2000, 2001), we derive $X(\text{HCO}) \sim 8 \times 10^{-10}$. The estimated $N(\text{HCO})/(\text{H}^{13}\text{CO}^+)$ abundance ratios in prototypical PDR range from 30, in the Orion Bar, to 3, in NGC 7023 (Schilke et al. 2001).

Altogether, the detection of widespread SiO and HCO emission in the starburst ring of NGC 1068 can be naturally explained by the chemical processing of molecular gas after a recent episode of star formation.

3.1.2. SiO emission in the circumnuclear disk (CND)

As is shown in Fig. 1, the spatial resolution of the 30 m in the 3–2 line ($19''$) guarantees that the SiO(3–2) emission detected toward the CND has little if any contamination from the starburst ring (of $\sim 30''$ diameter). The similar line-widths of the 2–1 and 3–2 SiO spectra at ($0''$, $0''$) provide further evidence that the bulk of the central SiO(3–2) emission comes from the CND. Furthermore, the linewidth of both SiO lines ($FWZP = 350 \text{ km s}^{-1}$) coincides with the total line width of the CO(1–0) emission integrated within the CND, as derived from the interferometer map of Schinnerer et al. (2000). While the SiO(3–2) line at ($0''$, $0''$) has no significant contribution from the starburst ring, the situation is less clear in the case of the SiO(2–1) spectrum: the $28''$ 30 m beam at half power may pick up emission coming mostly from the southern ridge of the star forming ring (see Fig. 1). Taking into account that the SiO(2–1) line temperatures measured over the ring are a factor of 2 lower than in the CND, the derived upper limit for the “alien” contribution to the SiO(2–1) CND spectrum is $\sim 25\%$, at most.

The $I(\text{SiO}(3-2))/I(\text{SiO}(2-1))$ ratio in the CND is of 0.7 ± 0.1 , once corrected for the contribution of the starburst ring to the 2–1 CND line ($\times 1/0.75$) and for the two-dimensional beam dilution of the CND ($\times (28''/19'')^2$). Simultaneously, we have evaluated the contribution of the CND to the SiO(2–1) spectra in the ring to be, at most, $\sim 25\%$. When we correct for this effect, the $I(\text{SiO}(3-2))/I(\text{SiO}(2-1))$ average ratio on the ring derived in Sect. 3.1.1 is raised to 0.5 ± 0.1 , i.e., a factor 1.5 smaller than the ratio in the CND. Although the difference is only marginal, it suggests that the excitation of SiO lines in the CND is different from that of the ring. In particular gas densities in the CND could be larger by a factor of ~ 4 compared to the starburst ring.

A relevant contribution from the molecular bar to the SiO emission detected at ($0''$, $0''$) is also very unlikely for several reasons. First, the bar hardly stands out in the HCN and CS interferometer maps of NCG 1068 (Tacconi et al. 1997): this is a relevant result, as the critical densities of HCN(1–0) and CS(2–1) lines are similar to that of SiO(2–1). Second, while weak CO emission is detected along the bar, it is significant only at $v < v_{\text{sys}}$: this is at odds with the observed SiO line profiles, roughly symmetric on both sides around v_{sys} .

Most remarkably, there is no evidence for significant recent star formation in the CND itself. Several multiwavelength criteria have classified the nucleus of NGC 1068 as a *pure* Seyfert nucleus, with little contribution from a nuclear starburst (MIR: Laurent et al. 2000; NIR: Imanishi 2002; Optical/Near-UV: Cid-Fernandes et al. 2001); the compact starburst emits $\leq 1\%$ of the total IR luminosity (Marco & Brooks 2003). The circumnuclear stellar population is concentrated in a 50 pc core of “post-starburst” intermediate age stars (age $\geq 5\text{--}16 \times 10^8$ yr) (Thatte et al. 1997).

We can exclude star formation either inside or outside the CND as the mechanism explaining the emission of SiO detected at ($0''$, $0''$). This poses the problem of the origin of SiO emission in the CND. The energy budget inside the CND seems to be largely dominated by the AGN itself; thus the

chemistry of molecular gas, in particular the silicon chemistry, could be driven by non-stellar processes. We discuss in Sect. 5.1 how the high abundances derived for SiO in the CND might be linked to the onset of XDR chemistry.

3.2. Emission of reactive ions in NGC 1068: The $\text{HOC}^+/\text{HCO}^+$ isomers

Detailed chemical models of XDR predict enhanced abundances of some reactive ions (e.g., H_3^+ , HCO^+ , SO^+ , CO^+ and HCNH^+) as well as related neutral species (such as CN and HCN) (Maloney et al. 1996; Black 1998a,b; Lepp & Dalgarno 1996). The tentative detection of CO^+ in the radio galaxy Cygnus A (Fuente et al. 2000) suggests that reactive ions may be used as an efficient diagnostic tool to study XDR chemistry in AGN. As part of this multi-species survey of NGC 1068, we have observed the 1–0 line of HCO^+ toward the CND. Most importantly, we have also searched for emission of its metastable isomer, HOC^+ . There is recent observational evidence that $X(\text{HCO}^+)/X(\text{HOC}^+)$ ratios, usually ranging from 300–6000 for dense molecular clouds in our Galaxy (Apponi et al. 1997, 1999), can reach values as low as 50–100 in UV-irradiated clouds (e.g., the prototypical PDR NGC 7023: Fuente et al. 2003). These results urged us to estimate the HCO^+ -to- HOC^+ ratio in the X-ray bathed environment of an AGN.

Figure 2 shows the $J = 1-0$ 30 m spectra of HCO^+ and HOC^+ observed toward the CND of NGC 1068. The emission of both species is detected. The interferometer HCO^+ map of Kohno et al. (2001) shows that the CND largely dominates the emission of HCO^+ in the inner 3 kpc of NGC 1068. Moreover, we can estimate a conservative upper limit for the contribution of the starburst ring to the HCO^+ emission detected at ($0''$, $0''$). Following the same procedure used in Sect. 3.1.2, here adapted to H^{13}CO^+ , we estimate that $<30\%$ of the ($0''$, $0''$) H^{13}CO^+ emission can be attributed to the starburst ring. We can reasonably extrapolate this estimate to HCO^+ . Additional evidence, similar to the one discussed in Sect. 3.1.2, supports that the 30 m HCO^+ spectrum is heavily dominated by emission coming from the CND.

The most remarkable result is the tentative detection of the $\text{HOC}^+(1-0)$ line, the first thus far obtained in an external galaxy. $\text{HOC}^+(1-0)$ emission is detected over 2σ levels in a 215 km s^{-1} velocity range ($\sim [-65 \text{ km s}^{-1}, +150 \text{ km s}^{-1}]$). The emission integrated within this velocity window reaches a 8.5σ significance level. The line profile of HOC^+ is noticeably asymmetrical with respect to v_{sys} : HOC^+ emission is mostly detected at *red* velocities. As is shown in Fig. 2, HCO^+ -to- HOC^+ intensity ratios for $v \geq v_{\text{sys}}$ range from ~ 40 to 100. These surprisingly low values rival the lowest values thus far derived in PDR. The low HCO^+ -to- HOC^+ intensity ratio measured in the CND of NGC 1068 suggests that the chemistry of molecular gas could be driven by the pervading X/UV irradiation coming from the Seyfert 2 nucleus. Most remarkably, the asymmetry of the HOC^+ line profile suggests that whatever causes the enhancement of this active ion, the process responsible seems to be unevenly efficient inside the CND. As it is discussed in Sect. 5.2, X-ray driven chemistry in the CND may

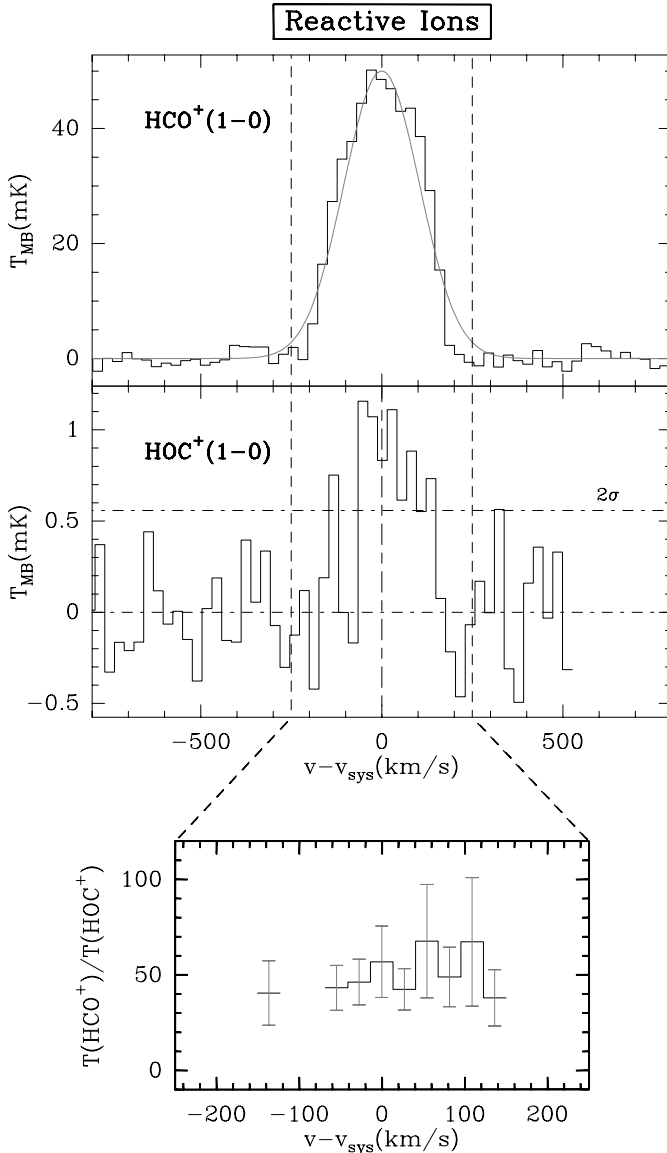


Fig. 2. *Top and middle:* $\text{HCO}^+(1-0)$ and $\text{HOC}^+(1-0)$ spectra of the CND of NGC 1068. *Bottom:* $\text{HCO}^+(1-0)$ -to- $\text{HOC}^+(1-0)$ temperature ratio profile derived for channels fulfilling $T[\text{HOC}^+(1-0)] > 2\sigma$. Error bars are $\pm\sigma$.

satisfactorily explain a dramatic change in the HCO^+ -to- HOC^+ abundance ratio.

3.3. CN emission in NGC 1068

CN is a high-dipole radical typically found in dense regions ($\sim 10^5 \text{ cm}^{-3}$). The abundance of CN is strongly linked to that of HCN. Theoretical models (Lepp & Dalgarno 1996) predict large CN-to-HCN abundance ratios (>1) in XDR. The comparison of the CN and HCN emission may thus provide a suitable diagnostic of the relevance of X-rays in the chemistry of the CND.

The CN(2–1) transition is split up into 18 hyperfine lines that appear blended into three groups at frequencies

$\sim 226.9 \text{ GHz}$, $\sim 226.7 \text{ GHz}$ and $\sim 226.4 \text{ GHz}$. We were able to observe the two most intense groups of the transition (the 226.9 GHz and 226.7 GHz groups, hereafter referred to as *high frequency* and *low frequency* respectively), although the *low frequency* group was only partially covered by the spectral bandwidth. The beam size at this frequency ($11''$) guarantees that the detected CN(2–1) emission must be coming from the CND.

The CN(2–1) spectrum is shown in Fig. 4 (main-beam temperature scaled to the CND; see Sect. 4.2). The measured high-frequency-to-low-frequency intensity ratio is below the expected value for the optically thin limit (high/low $\sim 1.64 \pm 0.14$ instead of 1.80). However, this estimate is hampered by the insufficient baseline coverage in the spectrum.

4. Molecular gas inventory of the CND

Understanding the peculiar chemistry of molecular gas revealed in the CND of NGC 1068 requires a global analysis of its molecular inventory. Furthermore, higher spatial resolution is key to extracting the maximum information from the 30 m spectra of SiO, HCO^+ and HOC^+ discussed above.

With this aim we have included in our analysis the information provided by published interferometer maps of NGC 1068 obtained for CO, CS and HCN (Schinnerer et al. 2000; Tacconi et al. 1994, 1997). These maps can help to improve our knowledge on the molecular abundances for species such as HCN or CS in the CND; due to their high spatial resolution, these observations are not hampered by source confusion between the CND itself and the starburst ring. In particular, the CO interferometer map allows us to estimate the molecular hydrogen column densities in the CND. Moreover, the spatio-kinematical information of the CO interferometer map is used for calculating the size and the location inside the CND of the gas components emitting at different velocities. Altogether, this information is employed in Sect. 4.3 to estimate via LVG models the abundances of several molecular species in the CND, separately, for the relevant velocity components.

4.1. Morphology of the CND: The interferometer CO(1–0) map

Figure 3 represents the CO(1–0) spatially integrated spectrum of the CND of NGC 1068. The line emission profile has been obtained by integrating the CO(1–0) interferometer data of Schinnerer et al. (2000) inside a $6'' \times 4''$ -rectangular region which contains the bulk of the CO emission in the CND. According to Schinnerer et al. (2000)'s estimates, we expect little zero-spacing flux missing in the CND integrated spectrum/map. Molecular gas in the CND is not evenly distributed around the AGN: two conspicuous knots (denoted as E[$1''$, $0''$] and W[$-1.5''$, $0''$] knots) form an asymmetrical ring around the AGN (see Fig. 1 of Schinnerer et al. 2000 and Fig. 1 in this work). The asymmetrical distribution of molecular gas in the CND is reflected by the profile of Fig. 3: the CO(1–0) emission integrated for $v < v_{\text{sys}}$ (hereafter, called *blue* component) is ~ 2 times that measured for $v > v_{\text{sys}}$ (hereafter, called *red* component). As expected for a disk rotating around the AGN,

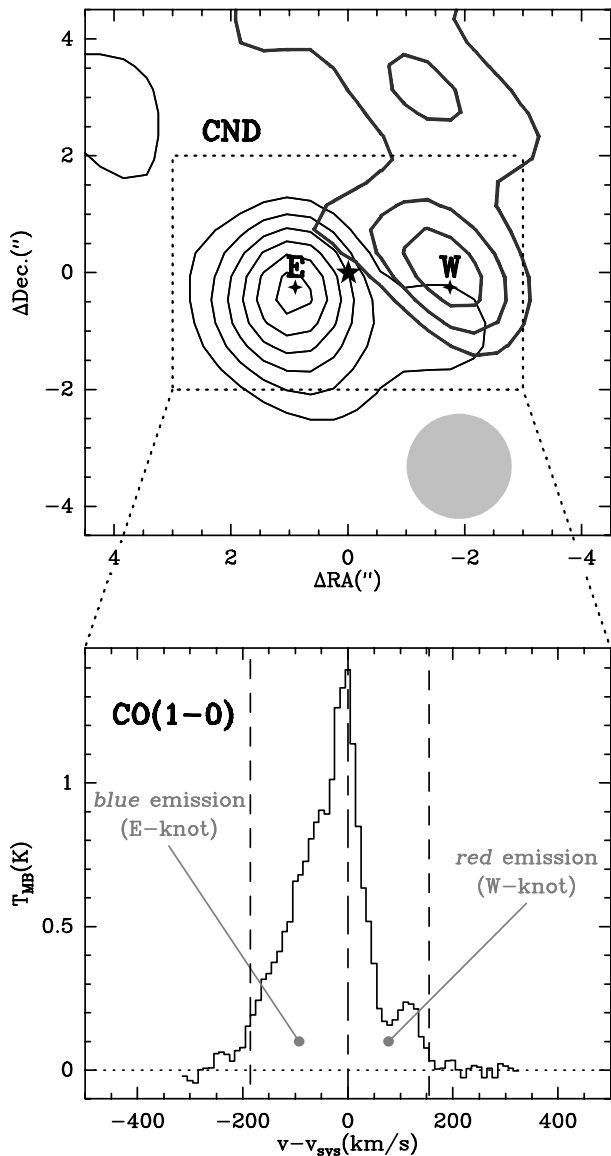


Fig. 3. *Top panel:* integrated intensity maps of CO(1–0) toward the CN of NGC 1068 obtained for the *blue* (thin contours: from 6σ by steps of 3σ ; $\sigma = 0.67 \text{ K km s}^{-1}$) and *red* (thick contours: same levels with $\sigma = 0.47 \text{ K km s}^{-1}$) emission components as defined in text (see also bottom panel). The maps have been derived from the data of Schinnerer et al. (2000). The starred marker highlights the AGN locus. *Bottom panel:* integrated spectrum of CO(1–0) emission in the CN. The W and E knots in the CO map correspond, respectively, to the *red* and *blue* components in the spectrum.

the emission coming from the E and W knots roughly correspond, respectively, to the *blue* and *red* components defined above. This is illustrated in Fig. 3.

The full sizes of the E and W knots, deconvolved by the $1.8'' \times 1.8''$ beam, are alike: $FWZP \approx 2.2''$. Therefore we deduce similar areas for the *blue* and *red* emitting regions: $\Omega_{\text{source}} \approx \pi \times 1.1^2 \text{ arcsec}^2 = 3.8 \text{ arcsec}^2$.

4.2. Molecular line profiles of the CN

Figure 4 displays all the molecular lines observed in this work toward the CN of NGC 1068. This includes the 30 m

Table 3. Integrated intensities of the spectra of Fig. 4 in the blue (Col. 2) and red (Col. 3) components. Column 4 = blue-to-red (east-to-west) ratio of mean temperatures. Errors (in brackets) are $1-\sigma$.

Transition	$I_{\text{blue}} (\text{K km s}^{-1})$	$I_{\text{red}} (\text{K km s}^{-1})$	$R_{E/W}$
CO(1–0)	127.1 (0.9)	60.1 (0.9)	1.77 (0.03)
CO(2–1)	95.5 (0.4)	51.2 (0.3)	1.56 (0.01)
CS(2–1)	8.7 (0.6)	3.2 (0.5)	2.24 (0.40)
HCN(1–0)	121.5 (1.7)	91.1 (1.5)	1.12 (0.02)
SiO(2–1)	8.5 (0.8)	6.2 (0.7)	1.15 (0.18)
SiO(3–2)	4.7 (0.5)	2.5 (0.4)	1.55 (0.32)
$\text{H}^{13}\text{CO}^+(1-0)$	6.3 (0.8)	6.9 (0.7)	0.77 (0.13)
$\text{HCO}^+(1-0)$	167.2 (2.2)	158.4 (2.1)	0.88 (0.02)
$\text{HOC}^+(1-0)$	2.1 (0.5)	2.8 (0.4)	0.61 (0.17)

spectra of SiO, HOC^+ , HCO^+ , H^{13}CO^+ and CN (panels 4–9 in Fig. 4). Temperatures have been rescaled assuming that the emission comes from the $6'' \times 4''$ -rectangular region containing the CN. Furthermore, we represent in panels 1–3 of Fig. 4, the CN spectra of CO, CS and HCN obtained from published interferometer maps. Similarly to CO (see Sect. 4.1), these CN spectra have been obtained by integrating the HCN and CS emission inside the $6'' \times 4''$ rectangular region which contains the bulk of the CN flux in both interferometer maps. We can redefine more precisely what we call *red* and *blue* velocities, ascribed, as argued above, to the W and E knots, respectively: based on the observed molecular profiles of Fig. 4, most of the molecular emission detected at *red* (*blue*) velocities for all species arises within the interval $0 < v - v_{\text{sys}} < 155 \text{ km s}^{-1}$ ($-185 \text{ km s}^{-1} < v - v_{\text{sys}} < 0$). Integrated intensities in the blue and red components of the spectra are listed in Table 3.

There are noticeable differences between the line shapes of the CN spectra shown in Fig. 4. We find line profiles dominated by emission at *blue* velocities for CO and CS, while line profiles of HCO^+ , H^{13}CO^+ and HOC^+ are dominated by *red* emission. As argued in Sect. 3.2, HOC^+ represents an extreme case as the bulk of the HOC^+ emission is detected at *red* velocities. HCN profiles are rather symmetrical with respect to v_{sys} . Finally, the SiO line profiles represent a case somewhat intermediate between HCN and CO. These differences are quantified in Fig. 4 and Table 3, which show the *blue-to-red* (east-to-west) average brightness temperature ratio ($R_{E/W}$) for all the CN spectra (except for CN(2–1), for which the determination of the blue and red components is hampered by the partial blending of the lines). $R_{E/W}$ ranges from 2.2 ± 0.4 (CS(2–1)) to 0.6 ± 0.2 ($\text{HOC}^+(1-0)$), i.e., from one extreme to the other, this ratio changes by a significant factor (~ 4) among the observed molecules. Figure 5 also illustrates this result: the HCN(1–0)/CO(1–0) temperature ratio is a factor of 2–3 larger for the red component than for the blue component. Furthermore, the CO(2–1)/CO(1–0) ratio profile, shown in Fig. 5, is also

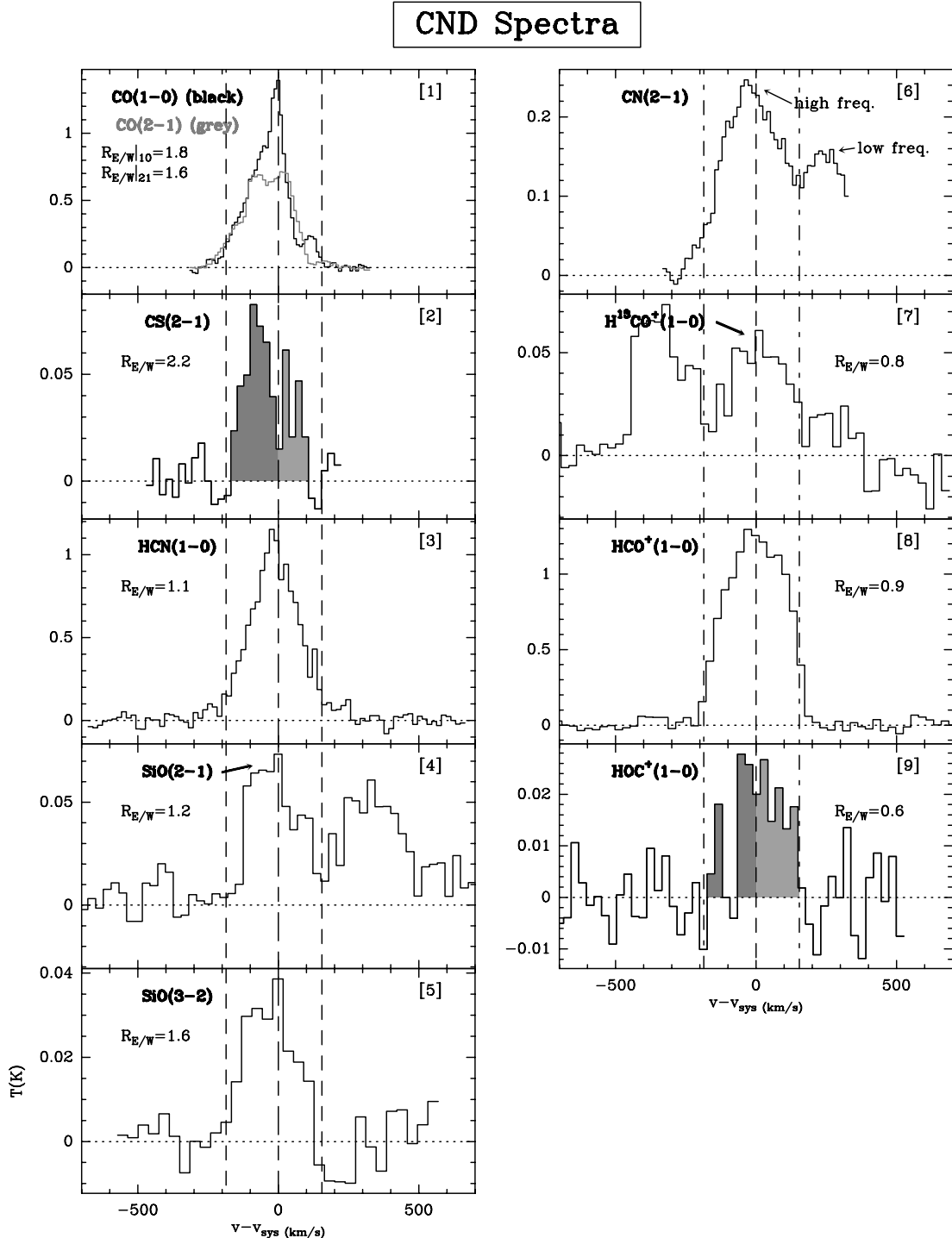


Fig. 4. Molecular lines in the CND. Sub-panels are labeled with the name of the line displayed. Sub-panels 1 to 3 are derived from interferometer data (Tacconi et al. 1994, 1997; Schinnerer et al. 2000); panels 4 to 9 show single-dish spectra observed towards the nucleus (temperatures corrected by dilution effects assuming that the emission is coming from the CND). Two vertical point-dashed lines at $v - v_{\text{sys}} = -185 \text{ km s}^{-1}$ and 155 km s^{-1} , delimit the *blue* and *red* kinematical components. For each line, the blue-to-red (east-to-west) average brightness temperature ratio ($R_{E/W}$) is indicated.

asymmetrical with respect to v_{sys} : the (2–1)-to-(1–0) ratio reaches higher-than-one values within a 70 km s^{-1} interval at *red* velocities, while it oscillates between 0.6 and 0.8 for the *blue* component.

Taken together, these results suggest that there is a chemical differentiation between the E and W knots of the CND.

4.3. Molecular gas abundances in the CND

4.3.1. LVG models

We have used single-component Large Velocity Gradient (LVG) models to estimate the column densities of the observed molecular species under certain assumptions which are the

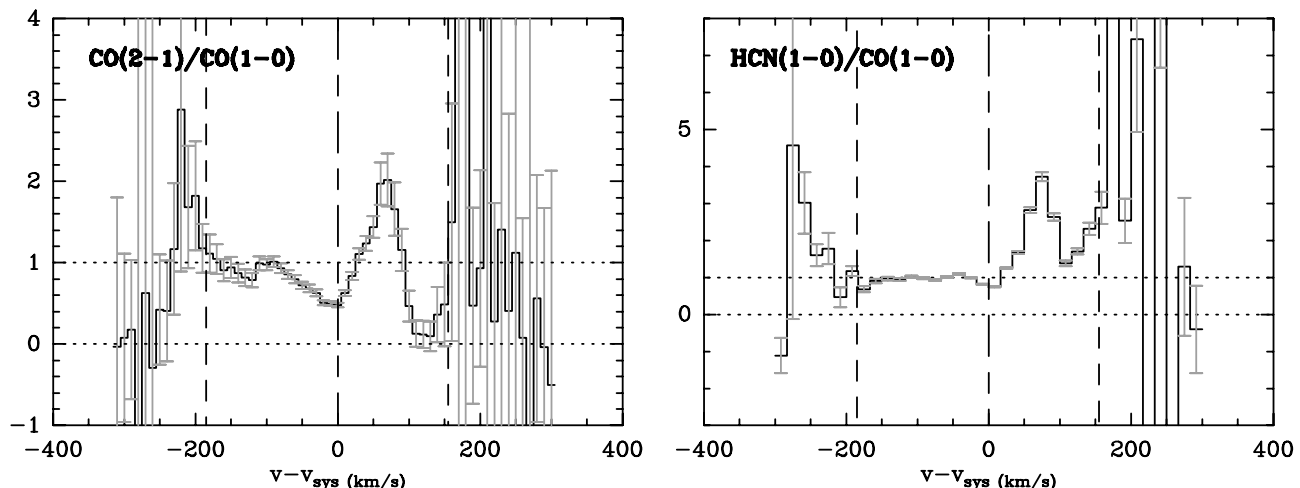


Fig. 5. Temperature ratio profiles derived from spectra of Table 4. The left panel shows the CO(2-1)-to-CO(1-0) ratio, and the right panel the HCN(1-0)-to-CO(1-0) ratio. Error bars are $\pm 3\sigma$.

basis of all our calculations. First, we assume that the kinetic temperature (T_K) of molecular gas in the CND is 50 K. This value was derived by Sternberg et al. (1994) from the LVG analysis of several CO emission-lines observed toward the CND. Therefore this value can be taken as a conservative lower limit for T_K . Furthermore, we adopt in our calculations an isotopic ratio of $^{12}\text{C}/^{13}\text{C} = 40$ (Wannier 1980).

It has been previously reported that LVG models of CO emission in PDR-type environments can lead to inconsistencies related to spatial fine structure, density and kinetic temperature (see the case of M 82 in Mao et al. 2000). However, high J -number transitions (out to CO($J = 7-6$)), not available for NGC 1068, are required to constrain LVG-parameters sufficiently to search for inconsistencies.

As argued in Sect. 4.1, the interferometric CO maps reveal two distinct knots (E–W) in the CND. These knots have similar sizes ($\Omega_{\text{source}} \sim 3.8 \text{ arcsec}^2$) and can be identified with two adjacent velocity components of emission in the spectra. As discussed in Sect. 4.2, the relative intensity ratio between these components depends on the molecular species. In our calculations we thus give our estimates of abundance ratios separately for the E/blue and W/red components. All source brightness temperatures ($T_S(\text{E/W})$), listed in Table 4, have been derived from the CND temperature scale used in Fig. 4, corrected by a dilution factor $f = \Omega_{\text{CND}}/\Omega_{\text{source}}$.

The range of LVG solutions ($n(\text{H}_2)$, $N/\Delta v$) are determined straightforwardly for SiO, CO, HCN and CN from the observed line ratios and the source brightness temperatures. In the case of SiO, we fit the (3-2)-to-(2-1) ratio and the 2-1 line source temperature. Correction for contamination from the ring is taken into account for SiO(2-1) (also for HCO⁺(1-0); see below). For CO and HCN we use the (4-3)-to-(1-0) line ratios and the 1-0 line source temperatures; 4-3 line temperatures of CO and HCN are derived from single-dish data published by Tacconi et al. (1994). In the case of CN, we fit the ratio of the two fine structure lines and the low-frequency line source temperature. However, and due to partial blending of the two fine groups, LVG solutions refer to global

Table 4. Mean temperatures in the East and West knots of the CND after correction for dilution: Col. 1 = name of the line; Col. 2 = mean temperature in the East-knot; Col. 3 = idem in the West-knot.

Transition	$\langle T \rangle_{\text{E}}(\text{K})$	$\langle T \rangle_{\text{W}}(\text{K})$
CO(1-0)	4.34	2.44
CO(2-1)	3.26	2.08
CO(4-3)	7.58	6.50
HCN(1-0)	4.15	3.71
HCN(4-3)	1.24	0.62
SiO(2-1)	0.29	0.25
SiO(3-2)	0.16	0.10
	$T_{\text{peak}}(\text{K})$	
CN(2-1, high freq.)	1.51	
CN(2-1, low freq.)	0.92	
HCO ⁺ (1-0)	5.73	6.50
H ¹³ CO ⁺ (1-0)	0.21	0.28
HOC ⁺ (1-0)	0.07	0.12
CS(2-1)	0.30	0.13

abundances with no distinction between red and blue velocity components. The LVG solution for H¹²CO⁺ is obtained by fitting both the H¹²CO⁺-to-H¹³CO⁺ temperature ratio measured for the 1-0 line and the H¹²CO⁺(1-0) source temperature. We have implicitly assumed that the derived density solution $n(\text{H}_2)$ can be considered as common for both H¹²CO⁺ and H¹³CO⁺. In the case of HOC⁺, LVG estimates are only obtained in the W knot, since the signal-to-noise ratio of the integrated emission at blue velocities (E knot) is too low (< 5). The estimate of $N/\Delta v$ for HOC⁺, only observed in the 1-0 line, rests on the assumption of a value for $n(\text{H}_2)$, here taken from H¹²CO⁺. This approach is justified as HOC⁺ and HCO⁺ are known to be formed/destroyed in chemical reactions taking place in the same gas clouds. Similarly, $N/\Delta v$ values for CS are derived assuming for this molecule the same gas density inferred from HCN in order to fit the CS(2-1) source brightness temperature.

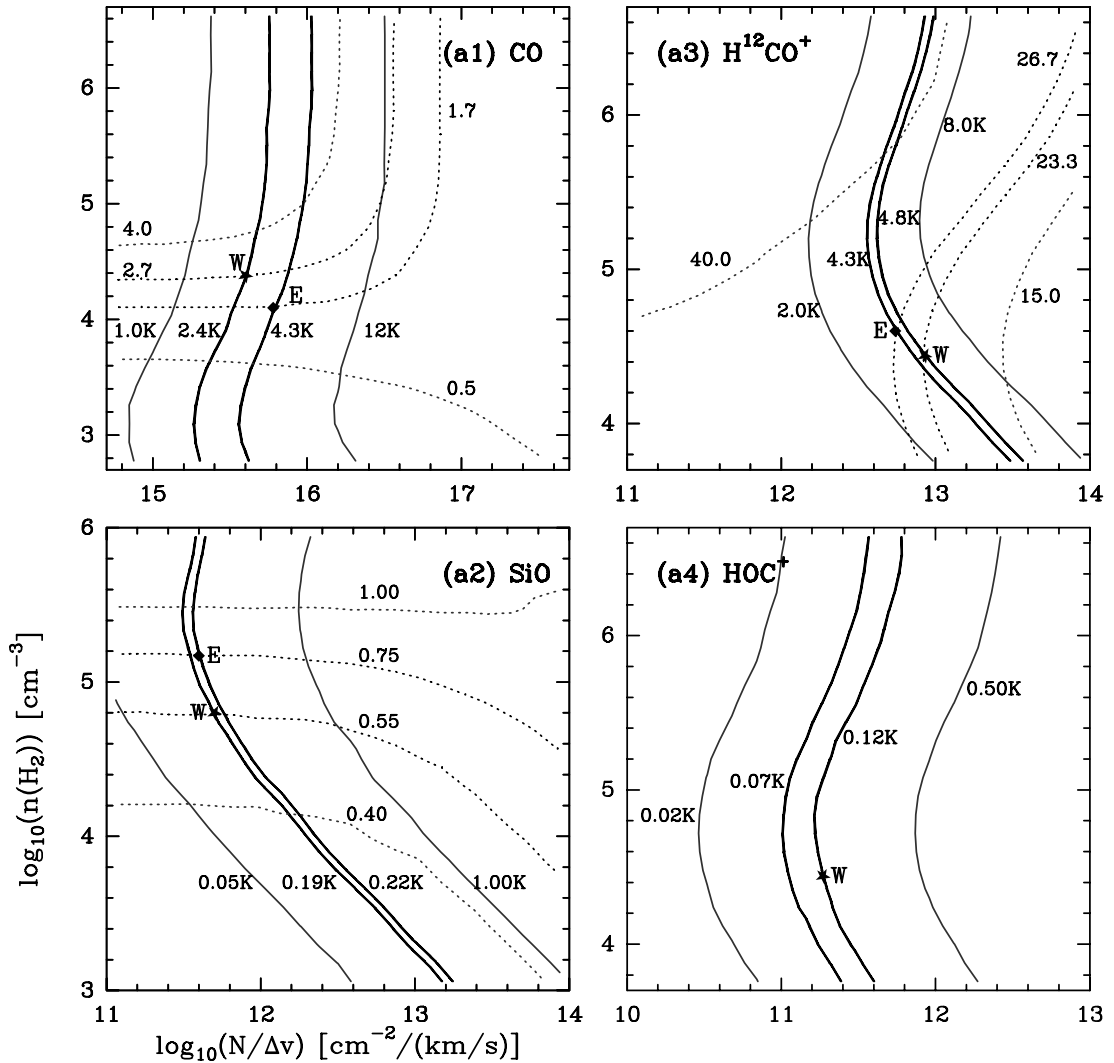


Fig. 6. LVG estimates for oxygenated species in the E/W knots of the CND. **a1)** For CO, continuous (pointed) curves are contours of constant 1–0 line temperature ((4–3)-to-(1–0) line ratio). **a2)** For SiO, same for 2–1 line temperature ((3–2)-to-(2–1) line ratio). **a3)** For H^{12}CO^+ , same for 1–0 line temperature ($[\text{H}^{12}\text{CO}^+]$ -to- H^{13}CO^+ 1–0 line ratio). **a4)** For HOC^+ , same for 1–0 line temperature. Squared (starred) markers show solutions for the East (West) knot.

Figures 6 and 7, and Table 5 summarize the results of LVG calculations for CO, HCN, CS, CN, SiO, HCO^+ and HOC^+ . Normalized with respect to $N(\text{CO})$, the column densities of SiO, HCO^+ and HOC^+ (i.e., $N(\text{SiO})/N(\text{CO})$, $N(\text{HCO}^+)/N(\text{CO})$ and $N(\text{HOC}^+)/N(\text{CO})$) are ≥ 2 –3 larger in the W knot than in the E knot. In contrast, $N(\text{HCN})/N(\text{CO})$ and $N(\text{CS})/N(\text{CO})$ column density ratios are similar in the two knots within a 25% uncertainty. These abundance ratios are reflecting the asymmetries of the spectra discussed in Sect. 4.2, suggestive of an uneven processing of molecular gas in the CND.

As a byproduct of LVG models for CO, we have estimated the $X \equiv N(\text{H}_2)/I(\text{CO})$ conversion factor for the molecular gas in the CND. Assuming a range of abundance ratios $[\text{CO}]/[\text{H}_2] \sim 5 \times 10^{-5}$ – 10^{-4} , we infer a X value of 3 – $6 \times 10^{19} \text{ cm}^{-2}/(\text{K km s}^{-1})$, i.e., ~ 4 – 8 times smaller than the canonical value $X = 2.2 \times 10^{20}$ (Solomon & Barrett 1991). Unless CO is underabundant by a similar factor (a scenario

invoked by Sternberg et al. 1994 in the oxygen depletion models clearly invalidated by the results of our work; see Sect. 5) we conclude that the X conversion factor is lower in the CND of NGC 1068. Similar deviations have been previously reported in other galactic central regions (Dahmen et al. 1998, and references therein). This might reflect the failure of some of the basic hypothesis that support the canonical value. In particular, the strong gravitational forces near galactic nuclei may prevent molecular clouds from reaching virialization.

5. Chemistry of molecular gas in the CND of NGC 1068

To give further insight into the chemistry of molecular gas in the CND we have compared, for a common set of abundance ratios, the values measured in NGC 1068 with those observed in a *reference* galactic region. Here we take as “zero-point” environment the “Extended Ridge” of OMC-1 (OER)

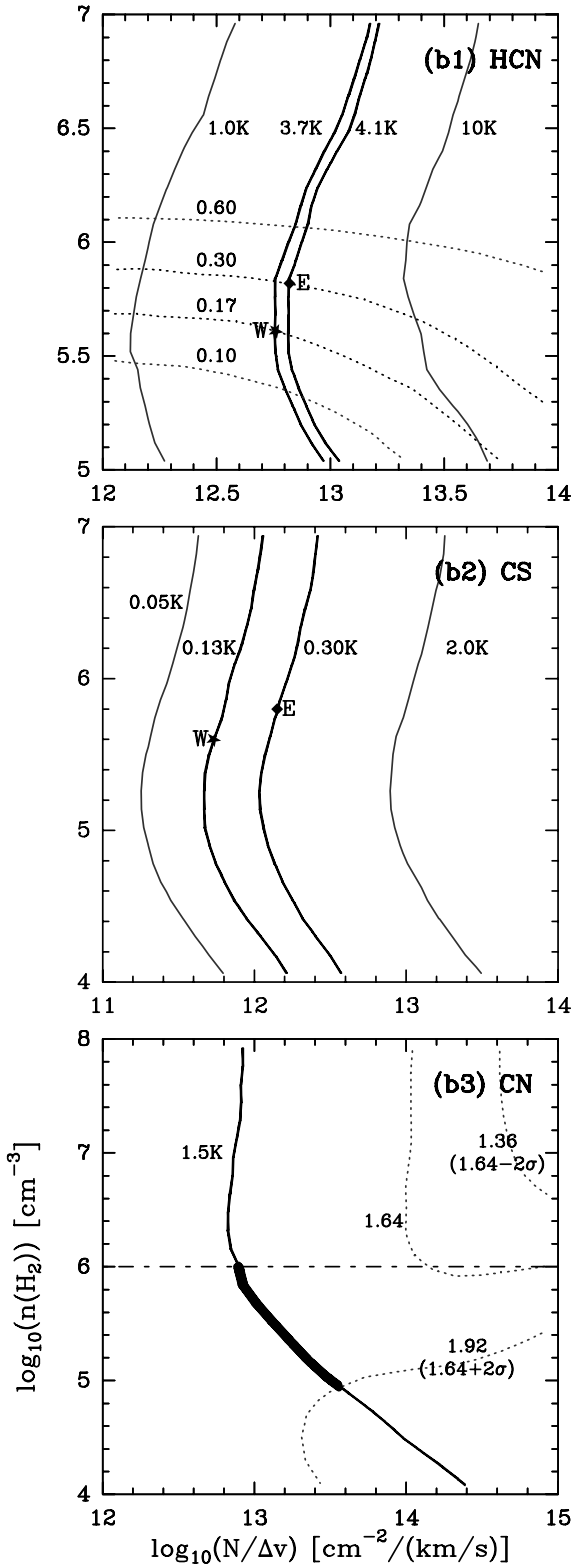


Fig. 7. LVG estimates for non-oxygenated species in the E/W knots of the CND. **b1)** For HCN, continuous (pointed) lines are contours of constant 1–0 line temperature ((4–3)-to-(1–0) line ratio). **b2)** For CS, same for 2–1 line temperature. **b3)** For CN, same for 2–1/high freq. line temperature ((2–1/high freq.)-to-(2–1/low freq.) ratio); a range of possible solutions found is highlighted in bold face: we impose $n(\text{H}_2) < 10^6 \text{ cm}^{-3}$ for consistency with the results from others species and allow for a $\pm 2\sigma$ uncertainty in the measured ratio. Markers are as in Fig. 6.

Table 5. LVG results: Col. 1 = chemical species; Col. 2 = parameters determined from the LVG models (n : molecular gas densities in cm^{-3} ; $N/\Delta v$: column densities per velocity interval in $\text{cm}^{-2} \text{ km}^{-1} \text{ s}$; X : chemical abundances relative to H_2 ; we assume $X(\text{CO}) = 8 \times 10^{-5}$ and compute the rest of abundances accordingly from column density ratios relative to CO); Col. 3 = solutions for the East-knot; Col. 4 = same for the West-knot; Col. 5 = east-to-west ratio of abundances.

Species	LVG-sol.	E/blue	W/red	$N_{\text{E/W}}$
CO	n	1.3×10^4	2.5×10^4	
	$N/\Delta v$	6.3×10^{15}	4.0×10^{15}	1.0
	X	8.0×10^{-5}	8.0×10^{-5}	
SiO	n	1.6×10^5	6.0×10^4	
	$N/\Delta v$	4.0×10^{11}	5.0×10^{11}	0.5
	X	5.1×10^{-9}	1.0×10^{-8}	
HCO ⁺	n	4.0×10^4	2.5×10^4	
	$N/\Delta v$	5.0×10^{12}	8.0×10^{12}	0.4
	X	6.3×10^{-8}	1.6×10^{-7}	
HOC ⁺	n	–	2.5×10^4	
	$N/\Delta v$	–	2.0×10^{11}	–
	X	–	4.0×10^{-9}	
HCN	n	6.3×10^5	4.0×10^5	
	$N/\Delta v$	6.3×10^{12}	5.0×10^{12}	0.8
	X	8.0×10^{-8}	1.0×10^{-7}	
CS	n	6.3×10^5	4.0×10^5	
	$N/\Delta v$	1.6×10^{12}	8.0×10^{11}	1.2
	X	2.0×10^{-8}	1.6×10^{-8}	
CN		<i>(global values)</i>		
	n	$> 1.6 \times 10^5$		
	$N/\Delta v$	$1-5 \times 10^{13}$		–
	X	$9 \times 10^{-8} - 5 \times 10^{-7}$		

(Blake et al. 1987), a relatively quiescent molecular region whose chemistry has been described as intermediate between the one typical of cold dark clouds and that of warm cores (Sutton et al. 1995). The choice of the OER as a *reference* region is also motivated by the similarity of physical parameters of molecular gas density ($n(\text{H}_2) \sim 10^4 - 10^5 \text{ cm}^{-3}$) and kinetic temperature ($T_{\text{K}} \sim 50 \text{ K}$) in the CND and in the OER. Therefore, significant differences in the abundance ratios of “critical” tracers between the CND and the OER can be mostly attributed to different chemistries being at work in these regions. We will also use the OER as the “zero point” basis to extrapolate the abundance ratios in the case of oxygen depletion models (Ruffle et al. 1998).

We list in Table 6 the following set of abundance ratios: $N(\text{HCN})/N(\text{CO})$, $N(\text{CS})/N(\text{CO})$, $N(\text{HCN})/N(\text{HCO}^+)$, $N(\text{CN})/N(\text{HCN})$, $N(\text{SiO})/N(\text{CO})$ and $N(\text{HCO}^+)/N(\text{HOC}^+)$. These abundance ratios can be significantly different depending on the chemical environment. As argued below, an evaluation of these ratios allows us to compare the chemical status of the CND and the OER with the predictions of models invoking either oxygen-depletion or X-ray driven chemistry:

- Our observations provide new constraints for oxygen-depletion models first proposed by Sternberg et al. (1994)

Table 6. Abundance ratios predicted/observed in different molecular regions: the E-knot of the CND of NGC 1068, same for the West-knot; a prototypical XDR (Lepp & Dalgarno 1996; Yan & Dalgarno 1997), the Orion Extended Region (OER) (Blake et al. 1987), and the OER corrected with oxygen depletion (Ruffle et al. 1998).

Abundance ratios	CND(E/blue)	CND(W/red)	XDR	OER	OER+oxygen depletion (Gas phase model)
HCN/CO	1.0×10^{-3}	1.2×10^{-3}	5×10^{-4}	1.0×10^{-4}	1×10^{-3}
CS/CO	2.5×10^{-4}	1.6×10^{-4}	$1-5 \times 10^{-4}$	5.0×10^{-5}	7×10^{-5}
HCN/HCO ⁺	1.3	0.6	0.5-1	2.2	25
CN/HCN	1-5 (<i>global value</i>)		3	0.7	20
SiO/CO	6.4×10^{-5}	1.2×10^{-4}	–	$<6.6 \times 10^{-6}$	–
HCO ⁺ /HOC ⁺	–	50	–	–	–

as an explanation for the high HCN/CO ratio measured in the CND of NGC 1068. This scenario is supported by X-ray and ultraviolet observations of the hot-ionized gas in the narrow-line region of NGC 1068 (Marshall et al. 1993; Ogle et al. 2003). With the inclusion of dust-grain chemistry in time-dependent models, Shalabiea & Greenberg (1996) were able to fit at “early times” ($t \approx 10^6$ yr) $\text{HCN/CO} \sim$ a few 10^{-3} with values less restrictive for the oxygen depletion. The overall consequences of selective oxygen-depletion in the chemistry of molecular clouds have been more extensively studied in the framework of gas-phase (Terzieva et al. 1998; Ruffle et al. 1998) and gas-grain chemical models (Shalabiea 2001). The primary effect of an oxygen underabundance is a reduced formation of CO. The fraction of carbon not consumed in the CO synthesis is then increased and it can thus enhance the abundances of some carbonated species, such as HCN, CS or CN; on the contrary, abundances of oxygen-bearing species are expected to be lower. This decrease is less important for HCO⁺, as in this case a lower oxygen abundance is mostly balanced by the increase of available carbon.

As shown in Table 6, the measured HCN/CO ratio in the CND of NGC 1068 (\sim a few 10^{-3}) is 1 order of magnitude larger than that derived for the OER. Oxygen depletion models can fit the HCN-to-CO ratio of the CND with an oxygen depletion of $[\text{O}]_{\text{CND}}/[\text{O}]_{\text{OER}} \sim 1/2$. However, this value of oxygen depletion would lead to large HCN/HCO⁺ ratios (\sim 25) which are at odds with the low ratios (\sim 1) of the CND. Furthermore, these models predict a significant enhancement of CN due to the reduction of O I which is an important source of CN destruction (Bachiller et al. 1997). Here also the CN-to-HCN ratio in the oxygen depletion models solution (\sim 20) is nearly one order of magnitude larger than the CND ratio (\sim 1–5, i.e., slightly above the OER standards). Finally, the predicted variation for the CS/CO ratio is marginal ($\times 1.4$) in the adopted oxygen-depletion solution, leading to values similar to that reported for the CND: $\text{CS/CO} \sim 2 \times 10^{-4}$.

- Lepp & Dalgarno (1996) proposed an alternative explanation of the high HCN/CO ratio measured in the CND of NGC 1068: X-rays coming from the central engine may significantly enhance the abundance of HCN in the neighbouring molecular gas. Thus, the HCN/CO ratio measured in NGC 1068 can be easily accounted for. In a XDR

chemistry some diatomic species, such as CN and OH are particularly robust (Lepp & Dalgarno 1996). Moreover, large abundances of OH favour the formation of CO⁺ and H₂O (Sternberg et al. 1996); these species take part directly in the production of large quantities of HCO⁺. The abundances of HCN, CN and HCO⁺ simultaneously reach their peak values at similar depths inside XDR (Yan & Dalgarno 1997). The XDR model of Yan & Dalgarno (1997) predicts an average CS/CO abundance ratio of $1-5 \times 10^{-4}$ for the range of depths inside the XDR that are expected to dominate the emission of molecular gas. As summarized in Table 6, the HCN/CO, HCN/HCO⁺, CN/HCN and CS/CO abundance ratios predicted by XDR models (see Lepp & Dalgarno 1996 for the three first ratios; the CS/CO ratio has been estimated from Yan & Dalgarno 1997) are in close agreement with the corresponding values estimated for the CND of NGC 1068.

In summary, while oxygen depletion models are able to fit the HCN/CO ratio measured in the CND of NGC 1068, the adopted solution leads to HCN/HCO⁺ and CN/HCN abundance ratios which are excessively large compared to that actually measured for the CND. In contrast, the models invoking XDR chemistry explain naturally the ratios measured in NGC 1068; these values depart significantly from the standard reference values of the OER. In the following sections we discuss how the detection of high abundances of SiO and HCO⁺ in the CND of NGC 1068 adds supporting evidence to the XDR chemistry scenario.

5.1. SiO in XDR

As is shown in Table 6, the SiO-to-CO abundance ratio measured toward the CND of NGC 1068 is high by normal galactic standards: $N(\text{SiO})/N(\text{CO}) \sim 6 \times 10^{-5} - 1.2 \times 10^{-4}$. The normalized SiO column densities toward the CND are at least one order of magnitude larger than the upper limit derived for the OER ($< 7 \times 10^{-6}$). Assuming an absolute abundance for CO of $X(\text{CO}) = 8 \times 10^{-5}$, this implies $X(\text{SiO}) = 5 \times 10^{-9} - 1.0 \times 10^{-8}$. As discussed in Sect. 3.1.1, a significant enhancement of SiO in molecular gas has been attributed to heavy shock processing of grains in starburst galaxies where values of $X(\text{SiO})$ up to a few 10^{-10} have been reported on scales of several hundred pc (García-Burillo et al. 2000, 2001). The CND

abundances of SiO estimated here are significantly larger than those reported for starbursts, however; this is further evidence that silicon chemistry in the CND is not being driven by star formation. In contrast, the estimated SiO abundances in the starburst ring of NGC 1068 ($X(\text{SiO}) \sim 2\text{--}3 \times 10^{-10}$) are in close agreement with SiO abundances measured in starbursts on similar spatial scales.

Alternatively, it has been suggested that X-ray irradiated dust grains can enhance silicon chemistry in gas phase. X-rays are able to heat very small silicate grains (10 Å), subsequently leading to their evaporation and to an enlargement of the Si gas-phase fraction (Voit 1991). Most remarkably, the nucleus of NGC 1068 shows a strong Fe K α line (Ogle et al. 2003 and references therein). The bulk of the 6.4 keV line of Fe I most likely comes from fluorescence in the Compton-thick molecular gas torus of NGC 1068. The detection of strong Fe K α line emission is therefore an indication that large column densities of molecular gas are being processed by X-rays. In a precedent study, Martín-Pintado et al. (2000) found a correlation between the intensity of the Fe 6.4 keV line and the derived abundance of SiO in the Sgr A and Sgr B molecular complexes at the Galactic Center.

5.2. HOC^+ in XDR

According to the estimates of Sect. 4.3, HOC^+ abundances derived for the CND of NGC 1068 are the largest ever measured in interstellar medium: $X(\text{HCO}^+)/X(\text{HOC}^+) \sim 30\text{--}80$. These low ratios are in direct contrast with those typically measured in galactic dense molecular clouds where values from ~ 6000 to ~ 300 have been reported thus far (Apponi et al. 1997, 1999). Most interestingly, the lowest value found by Apponi et al. (1999) corresponds to the Orion bar, a prototypical PDR. Very low ratios ($\sim 50\text{--}120$) have been recently found in the prototypical PDR NGC 7023 (Fuente et al. 2003). As argued below, we propose that low $R \equiv X(\text{HCO}^+)/X(\text{HOC}^+)$ ratios can be explained for molecular clouds with high ionization degrees, either in XDR or in PDR.

The fast hydrogen-catalyzed isomerization of HOC^+ into HCO^+ usually shifts the equilibrium between both species towards significantly lower abundances of HOC^+ . However, as suggested by Smith et al. (2002), the isomerization process converting HOC^+ into HCO^+ could be compensated by the destruction of HCO^+ due to interaction with electrons. This process is likely to be enhanced at high electron densities ($X(e^-) \sim 10^{-5}$). The latter could explain why the lowest R values have been measured in galactic PDR (Apponi et al. 1999; Fuente et al. 2003). Furthermore, the $X(\text{HCO}^+)/X(\text{HOC}^+)$ ratio at equilibrium is also sensitive to the dominant mechanism of $\text{HCO}^+/\text{HOC}^+$ formation: the more efficient is the relative production of HOC^+ , the lower is the ionization degree required to reach a certain R ratio. Typical paths for the formation of $\text{HCO}^+/\text{HOC}^+$ are (Apponi et al. 1997 and references therein):

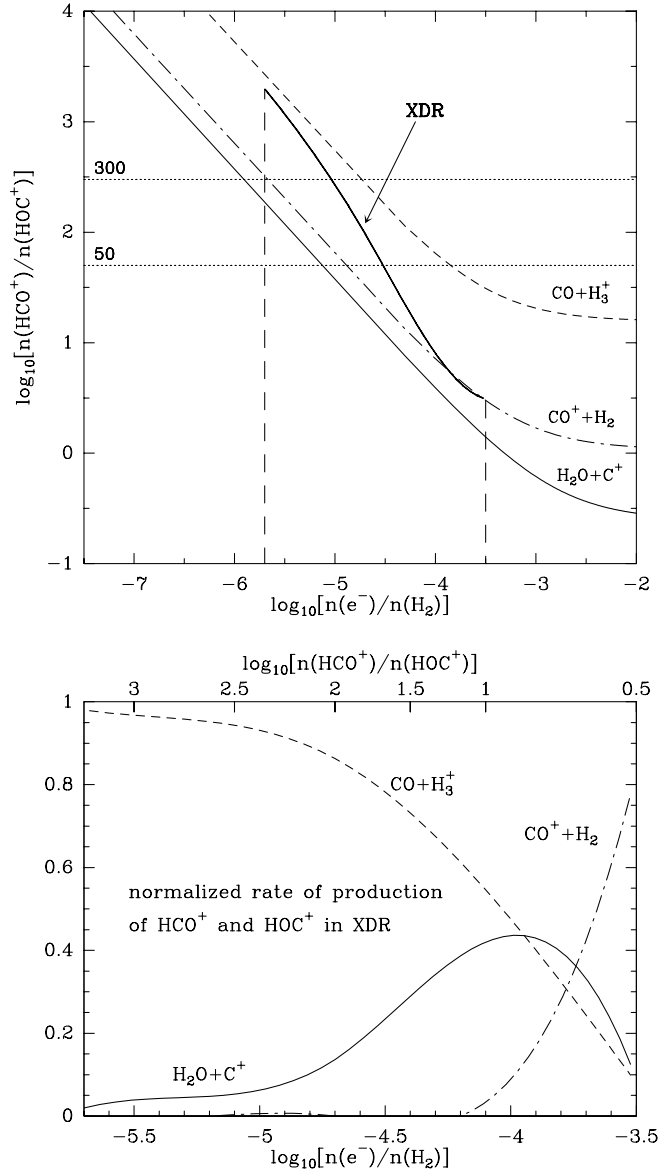
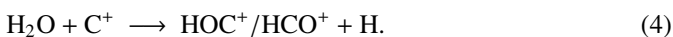
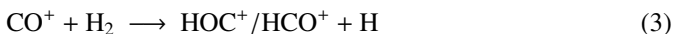
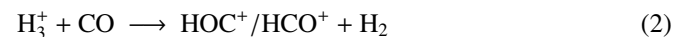


Fig. 8. *Top panel:* steady state HCO^+ -to- HOC^+ abundance ratio as a function of the ionization degree of molecular gas. Curves for single formation paths are plotted; the thick line shows the predicted ratio for a XDR chemistry. *Bottom panel:* fraction of HCO^+ and HOC^+ molecules formed along each chemical path in a XDR chemistry.

The branching ratio for the net production of nascent HOC^+ , hereafter denoted by α , depends on the particular formation pathway. The value of α is 0.06 for reaction 2, 0.48 for 3 and 0.8 for 4. In a real case scenario the three reactions coexist, and thus the equivalent branching ratio, α_{eff} , is an average of the individual α , weighted by the fraction of HCO^+ and HOC^+ particles that are actually formed following a certain pathway. We have derived how R depends on the ionization degree of molecular gas, separately, for the different reactions, assuming the rate coefficients given by Smith et al. (2002) (Fig. 8, top panel). We find that in order to obtain values of $R \sim 50\text{--}300$ high ionization degrees are needed: $X(e^-) \sim 10^{-6}\text{--}10^{-4}$. These high electronic abundances are typically reached in XDR

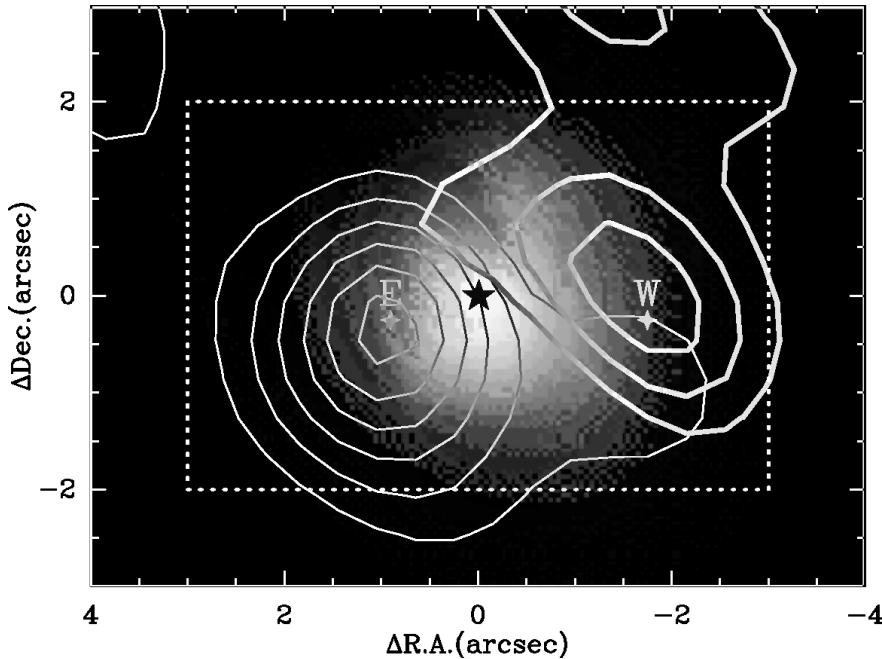


Fig. 9. X-ray emission and molecular gas in the CND: overlay of the distribution of hard X-ray emission in the 6–8 keV band (gray scale adapted from Ogle et al. 2003: whiter shades stand for stronger emission) and the CO(1–0) integrated emission as in Fig. 3. The AGN locus is highlighted by the starred marker.

(Lepp & Dalgarno 1996; Maloney et al. 1996). Figure 8 illustrates also the relation between the dominant formation path and the isomer ratio: less extreme ionization degrees are needed to reach low R ratios if the predominant reaction has a large α . On the other hand, much higher ratios ~ 300 – 6000 , like that typically measured in molecular clouds, can be easily accounted for if electronic abundances approach standard levels $< 10^{-6}$ – 10^{-7} .

We have also derived the dependence of α_{eff} on the ionization degree for an adopted XDR model (see the curve for R in the top panel of Fig. 8). The abundances of all molecular species, contributing to (2)–(4), have been taken from Maloney et al. (1996), except for CO^+ , whose abundance curve is taken from the PDR model of Sternberg et al. (1995). Values of $R \sim 30$ – 80 , like that measured in the CND of NGC 1068, can be easily accounted for assuming an average ionization degree of $X(e^-) \sim 10^{-5}$ for the bulk of molecular gas.

The relative weight of the 3 formation paths of HOC^+ in a typical XDR is also represented, as a function of $X(e^-)$, in Fig. 8 (bottom panel). While reaction (2) clearly dominates the balance for $X(e^-) < 10^{-5}$, reactions involving H_2O (4) and CO^+ (3) are predominant for $X(e^-) > 10^{-4}$. Recent observations of galactic PDR (Fuente et al. 2003; Rizzo et al. 2003) have confirmed that low $\text{HCO}^+/\text{HOC}^+$ ratios are indeed correlated with large abundances of CO^+ and/or H_2O .

5.3. Anisotropic X-ray illumination of the CND?

The results of this work strongly favour an overall scenario where the CND of NGC 1068 has become a giant XDR. It is tempting to speculate if X-ray driven chemistry can also explain the mild but systematic differences in the molecular abundances of SiO , HCO^+ , HOC^+ and HCN between the E and the W knots of the CND. Figure 9 shows the distribution of X-ray emission inside the 6–8 keV band in the CND

of NGC 1068 (adapted from Ogle et al. 2003). X-ray emission in this energy band is dominated by the Fe I $K\alpha$ line at 6.4 keV in NGC 1068. There is a $10''$ extended emission (not shown in Fig. 9) which corresponds to the ionization cones. The strongest component, however (shown in Fig. 9), should be tracing the illuminated inner wall of the CND torus. Most interestingly, this figure shows tantalizing evidence of a different degree of penetration of X-rays into the E/W knots: the western side of the molecular torus, corresponding to the inner wall of W knot, seems to be more illuminated than its eastern counterpart. This would be in agreement with the reported chemical differentiation seen between the E/W molecular knots. A difference in the attenuating column densities, estimated from CO, exists between the two CND knots: on 100 pc scales, $N(\text{H}_2)|_{\text{East}}/N(\text{H}_2)|_{\text{West}} \sim 2$. However, we do not know if these or even greater differences hold at smaller scales which are probably more relevant to probe X-ray absorption by neutral gas in the torus. In this context, it is however suggestive to note that the strongest H_2O megamasers, which are collisionally excited in the warmest region of the CND illuminated by X-rays (Neufeld et al. 1994), are mostly located in the western side of the molecular torus (Greenhill & Gwinn 1997).

High-resolution interferometer observations will give a sharp view of molecular abundance changes inside the CND at small scales for *critical* tracers such as SiO , CN and HOC^+ . A detailed comparison of these maps with the Chandra images of the CND may help to constrain this scenario.

6. Conclusions

We summarize the main results obtained in this work as follows:

- We report on the detection of significant $\text{SiO}(3-2)$ and $\text{SiO}(2-1)$ emission in the 200 pc circumnuclear disk of

NGC 1068. The large overall abundance of SiO in the CNL ($\sim(5-10)\times 10^9$) cannot be explained by shocks driven by star formation on molecular gas as there is counter-evidence of a recent starburst in the nucleus of NGC 1068. While SiO emission is also detected over the starburst ring, we estimate that SiO abundances there are 10 times lower than those measured in the CNL. These lower abundances of SiO are in close agreement with that measured in starbursts on similar spatial scales, however.

- We also report on the first extragalactic detection of the reactive ion HOC^+ . Most remarkably, the estimated $\text{HCO}^+/\text{HOC}^+$ abundance ratio in the nucleus of NGC 1068, $\sim 30-80$, is the smallest ever measured in molecular gas. The line profile of HOC^+ is markedly asymmetrical with respect to v_{sys} : HOC^+ emission is mostly detected at *red* velocities. Whatever process is responsible for the enhancement of this reactive ion, it seems to be unevenly efficient inside the CNL.
- Results from additional mm-observations have served for estimating abundances of CN, HCO^+ , HOC^+ , H^{13}CO^+ and HCO. These estimates are complemented by a re-evaluation of molecular abundances for HCN, CS and CO, based on previously published single-dish and interferometer observations of NGC 1068. While models invoking oxygen depletion in molecular gas successfully fit the HCN/CO ratio measured in the CNL, they fail to account for our estimates of the HCN/ HCO^+ and CN/HCN abundance ratios. On the contrary, XDR models can simultaneously explain these ratios. The detection of high abundances of SiO and HOC^+ in the CNL of NGC 1068 gives further support to the XDR chemistry scenario. The processing of 10 \AA dust grains by X-rays, as a mechanism to enhance silicon chemistry in gas phase, would explain the large SiO abundances of the CNL. Finally, we have shown that the low $\text{HCO}^+/\text{HOC}^+$ ratios measured in the CNL can be explained if molecular clouds have the high ionization degrees typical of XDR ($X(e^-) \sim 10^{-6}-10^{-4}$). An examination of the different formation paths of HOC^+ suggests that reactions involving H_2O and/or CO^+ would be the predominant precursors of HOC^+ in XDR.
- The XDR scenario could also provide an explanation for the different abundances of SiO, HCO^+ and, especially, of HOC^+ measured in the E and W knots. The Chandra images of the CNL in the 6–8 keV band, dominated by the emission of the Fe I $K\alpha$ line, show tantalizing evidence of a different degree of penetration of hard X-rays into the E and W knots. This suggests that larger columns of molecular gas are being processed by X-rays in the W knot.

Acknowledgements. We acknowledge the IRAM staff from Pico Veleta and Granada for help provided during the observations. We wish to thank A. Rodríguez-Franco for his support during the observations. We also wish to thank E. Schinnerer and L. J. Tacconi for providing their interferometer data. This research has made use of NASA's Astrophysics Data System (ADS) and the NASA/IPAC Extragalactic Database (NED). This paper has been partially funded by the Spanish MCyT under projects DGES/AYA2000-0927, ESP2001-4519-PE, ESP2002-01693, PB1998-0684, ESP2002-01627 and AYA2002-10113E.

References

- Apponi, A. J., Pesch, T. C., & Ziurys, L. M. 1999, *ApJ*, 519, L89
 Apponi, A. J., & Ziurys, L. M. 1997, *ApJ*, 481, 800
 Bachiller, R., Fuente, A., Bujarrabal, V., et al. 1997, *A&A*, 319, 235
 Blake, G. A., Sutton, E. C., Masson, C. R., & Phillips, T. G. 1987, *ApJ*, 315, 621
 Black, J. H. 1998a, *Faraday Discuss.*, 109, 257
 Black, J. H. 1998b, in *The Molecular Astrophysics of Stars and Galaxies*, ed. T. W. Hartquist, & D. A. Williams (Oxford: Oxford Univ. Press), 469
 Bland-Hawthorn, J., Gallimore, J. F., Tacconi, L. J., et al. 1997, *Ap&SS*, 248, 9
 Cid-Fernandes, R., Heckman, T., Schmitt, H., González-Delgado, R. M., & Storchi-Bergmann, T. 2001, *ApJ*, 558, 81
 Davies, R. I., Sugai, H., & Ward, M. J. 1998, *MNRAS*, 300, 388
 Dahmen, G., Hüttemeister, S., Wilson, T. L., & Mauersberger, R. 1998, *A&A*, 331, 959
 Fuente, A., Black, J. H., Martín-Pintado, J., et al. 2000, *ApJ*, 545, L113
 Fuente, A., Rodríguez-Franco, A., García-Burillo, S., Martín-Pintado, J., & Black, J. H. 2003, *A&A*, 406, 899
 Gallimore, J. F., Baum, S. A., O'Dea, C. P., & Pedlar, A. 1996a, *ApJ*, 458, 136
 Gallimore, J. F., Baum, S. A., & O'Dea, C. P. 1996b, *ApJ*, 464, 198
 García-Burillo, S., Martín-Pintado, J., Fuente, A., & Neri, R. 2000, *A&A*, 355, 499
 García-Burillo, S., Martín-Pintado, J., Fuente, A., & Neri, R. 2001, *ApJ*, 563, L27
 García-Burillo, S., Martín-Pintado, J., Fuente, A., Usero, A., & Neri, R. 2002, *ApJ*, 575, L55
 Genzel, R., Lutz, D., Sturm, E., et al. 1998, *ApJ*, 498, 579
 González-Delgado, R. M., Heckman, T., & Leitherer, C. 2001, *ApJ*, 546, 845
 Greenhill, L. J., & Gwinn, C. R. 1997, *Ap&SS*, 248, 261
 Helfer, T. T., & Blitz, L. 1995, *ApJ*, 450, 90
 Imanishi, M. 2002, *ApJ*, 569, 44
 Kohno, K., Matsushita, S., Vila-Vilaró, B., et al. 2001, in *The Central kpc of Starbursts and AGN: The La Palma Connection*, ed. J. H. Knapen, J. E. Beckman, I. Shlosman, & T. J. Mahoney, *ASP Conf. Ser.*, 249, 672
 Laurent, O., Mirabel, I. F., Charmandaris, V., et al. 2000, *A&A*, 359, 887
 Lepp, S., & Dalgarno, A. 1996, *A&A*, 306, L21
 Maloney, P. R., Hollenbach, D. J., & Tielens, A. G. G. M. 1996, *ApJ*, 466, 561
 Mao, R. Q., Henkel, C., Schulz, A., et al. 2000, *A&A*, 358, 433
 Marco, O., & Brooks, K. J. 2003, *A&A*, 398, 101
 Marshall, F. E., Netzer, H., Arnaud, K. A., et al. 1993, *ApJ*, 405, 168
 Martín-Pintado, J., de Vicente, P., Rodríguez-Fernández, N. J., Fuente, A., & Planesas, P. 2000, *A&A*, 356, L5
 Neufeld, D. A., Maloney, P. R., & Conger, S. 1994, *ApJ*, 436, L127
 Ogle, P. M., Brookings, T., Canizares, C. R., Lee, J. C., & Marshall, H. L. 2003, *A&A*, 402, 849
 Planesas, P., Gómez-González, J., & Martín-Pintado, J. 1989, *A&A*, 216, 1
 Planesas, P., Scoville, N., & Myers, S. T. 1991, *ApJ*, 369, 364
 Rizzo, J. R., Fuente, A., Rodríguez-Franco, A., & García-Burillo, S. 2003, *ApJ*, 597, L153
 Ruffle, D. P., Hartquist, T. W., Caselli, P., Rawlings, J. M. C., & Williams, D. A. 1998, *Ap&SS*, 262, 177
 Schenewerk, M. S., Snyder, L. E., & Hjalmarson, A. 1986, *ApJ*, 303, L71

- Schenewerk, M. S., Snyder, L. E., Hollis, J. M., Jewell, P. R., & Ziurys, L. M. 1988, *ApJ*, 328, 785
- Schilke, P., Pineau des Forêts, G., Walmsley, C. M., & Martín-Pintado, J. 2001, *A&A*, 372, 291
- Schinnerer, E., Eckart, A., Tacconi, L. J., Genzel, R., & Downes, D. 2000, *ApJ*, 533, 850
- Scoville, N. Z., Matthews, K., Carico, D. P., & Sanders, D. B. 1988, *ApJ*, 327, L61
- Shalabiea, O. M., & Greenberg, J. M. 1996, *A&A*, 307, 52
- Shalabiea, O. M. 2001, *A&A*, 370, 1044
- Smith, M. A., Schlemmer, S., von Richthofen, J., & Gerlich, D. 2002, *ApJ*, 578, L87
- Solomon, P. M., & Barrett, J. W. 1991, in *Proc. 146th Symp. IAU, Dynamics of Galaxies and Their Molecular Cloud Distributions*, ed. F. Combes, & F. Casoli (Dordrecht: Kluwer Academic Publishers), 235
- Sternberg, A., & Dalgarno, A. 1995, *ApJS*, 99, 565
- Sternberg, A., Genzel, R., & Tacconi, L. J. 1994, *ApJ*, 436, L131
- Sternberg, A., Yan, M., & Dalgarno, A. 1996, in *Molecules in Astrophysics: Probes and Processes*, ed. E. F. van Dishoeck (Dordrecht: Kluwer), IAU Symp., 178, 141
- Sutton, E. C., Peng, R., Danchi, W. C., et al. 1995, *ApJS*, 97, 455
- Tacconi, L. J., Gallimore, J. F., Genzel, R., Schinnerer, E., & Downes, D. 1997, *Ap&SS*, 248, 59
- Tacconi, L. J., Genzel, R., Blietz, M., et al. 1994, *ApJ*, 426, L77
- Terzieva, R., & Herbst, E. 1998, *ApJ*, 501, 207
- Thatte, N., Quirrenbach, A., Genzel, R., Maiolino, R., & Tecza, M. 1997, *ApJ*, 490, 238
- Voit, G. M. 1991, *ApJ*, 379, 122
- Wannier, P. G. 1980, *ARA&A*, 18, 399
- Yan, M., & Dalgarno, A. 1997, *ApJ*, 481, 296